Measurement of nanoplasmonic field enhancement with ultrafast photoemission

Péter Rácz[1,‡], Zsuzsanna Pápa,[2,3,‡], István Márton[1], Judit Budai[2,3], Piotr Wróbel[4], Tomasz Stefaniuk[4], Christine Prietl[5], Joachim R. Krenn[5] and Péter Dombi[1,2,]*

[1] MTA "Lendület" Ultrafast Nanooptics Group, Wigner Research Centre for Physics, 1121 Budapest, Hungary

[2] ELI-ALPS Research Institute, ELI-HU Nonprofit Kft., 6720 Szeged, Hungary

[3] Department of Optics and Quantum Electronics, University of Szeged, 6720 Szeged, Hungary

[4] Faculty of Physics, University of Warsaw, 02-093 Warsaw, Poland

[5] Institut für Physik, Karl-Franzens Universität Graz, 8010 Graz, Austria

[‡]these authors contributed equally

ABSTRACT Probing nanooptical near-fields is a major challenge in plasmonics. Here, we demonstrate an experimental method utilizing ultrafast photoemission from plasmonic nanostructures that is capable of probing the maximum nanoplasmonic field enhancement in any metallic surface environment. Directly measured field enhancement values for various samples are in good agreement with detailed finite-difference time-domain simulations. These results establish ultrafast plasmonic photoelectrons as versatile probes for nanoplasmonic near-fields.

KEYWORDS nanoplasmonics, field enhancement, ultrafast interactions, photoelectrons, femtosecond laser pulses

MANUSCRIPT TEXT

Nanoscale localization of electromagnetic fields in the vicinity of metal structures is a well-exploited phenomenon in many applications. It is especially advantageous to utilize either propagating surface plasmons at metal films or localized plasmons in metal nanoparticles to achieve substantial enhancement of the electric field of light in highly confined, nanoscale environments[1,2]. This field enhancement phenomenon is thus inherently connected to nanooptical field localization.

Scientific and technological applications of plasmonic field enhancement and/or localization include surface enhanced Raman scattering (SERS)[3,4], plasmonic biosensors[5,6], optoelectronics[7,8], photovoltaics[9], construction of ultrafast nanoemitters[10-13] and many more[14]. In spite of the immense importance of the field enhancement effect, its actual magnitude remains a highly debated issue due to the lack of accurate, direct and non-destructive experimental probes measuring and quantifying electromagnetic fields in nanometric volumes.

Raman signal enhancement together with well-known, simple signal scaling laws in SERS provided an early measure for plasmonic field enhancement[3,4]. More recently, indirect quantitative estimates show between 30 and 120 field enhancement factors for different nanostructured samples[15,16]. A similar concept based on two-photon photoluminescence signal levels confirmed field enhancement values of some dozens for gold nanostrip and bowtie geometries[17]. Alternatively, there are also other approaches that rely on irreversible changes induced by a critical value of the electric field such as (typically two-photon)

photopolymerization[18-20] and direct ablation[21] of nanopatterned samples with field enhancement estimates ranging from 34 to 600 for different geometries. In addition, a particularly high, three orders of magnitude enhancement was deduced based on the measurement of dc photocurrents in plasmonic sub-nm gaps[22]. Even though these methods provide sound quantitative estimates for plasmonic field enhancement, a general, locally sensitive, non-destructive probe providing a measurement instrument for the field enhancement of any nanopatterned metal surface would be of great benefit.

Therefore, here we demonstrate that ultrafast photoemission is a versatile tool for measuring the maximum plasmonic field enhancement in any metallic, nanostructured environment at a surface. Our results are corroborated by detailed finite-difference time-domain (FDTD) simulations of the experimentally probed geometries involving both localized and propagating plasmons without the use of fitting parameters.

Our experimental concept relies on the known facts that (i) nanooptical, plasmonic near-fields induce photoemission from metal surfaces[23-25] and nanoparticles,[26,27] and the resulting electron kinetic energy distribution can be easily measured; (ii) the electrons that acquire the highest kinetic energy in the nanolocalized field are the rescattered electrons,[28] and finally, (iii) there is a well-defined, simple relationship between the local field strength and the maximum electron kinetic energy, based on the ponderomotive acceleration mechanism of electrons[29,30]. Thus, by measuring the highest electron kinetic energy for a given plasmonic structure, the maximum hot-spot field enhancement can be extracted from the data, as electron spectral cutoff regions are composed of rescattered electrons that are directly sensitive to the nanooptical field maxima. This principle is valid provided that the quiver amplitude of the free electrons in the enhanced local field is much smaller than the plasmonic field decay length[31].

If the plasmonic photoemission process takes place at a certain phase of the oscillating, local electric field, the free, photoemitted electrons are driven back to the surface within roughly half of an oscillation cycle. At the metal surface, electrons can rescatter elastically with some probability, in complete analogy with the corresponding atomic physics process taking place after photoionization of an atom[28,29]. It can be rigorously proven that exactly these rescattered electrons acquire the highest kinetic energy in the cycle-by-cycle acceleration process in the oscillating, local field[29,30].

In experimental terms, it is only the rescattered electrons that contribute to the spectral cutoffs observed in the electron kinetic energy spectra. The maximum electron energy (Q_{max}) is given by the simple formula[29,30]

$$Q_{max} = 10.007\ e^2\lambda^2 E_{loc,max}^2 / (16\ \pi^2 mc^2) + 0.538\ W, \quad (1)$$

where m and e are the electron mass and charge, respectively, λ is the laser wavelength, E_{loc} is the local electromagnetic field, c is the speed of light and W is the work function of the metal. The prefactor 10.007 is based on a classical electron trajectory approach and can be derived by maximizing the kinetic energy for all electrons that backscatter fully elastically from the surface after photoemission and free electron motion[28-30]. The second term, 0.538 times the work function is a quantum mechanical correction to the classical approach[29]. Therefore, these prefactors are not empirical and they are universally valid irrespective of the experimental conditions.

Even though for the case of nanotips, field enhancement factors of up to 6 were reported by this approach[30], the main enhancement mechanism there is geometric and has apparently nothing to do with plasmon resonances. (Field enhancement results for gold and tungsten nanotips turned

out to be essentially the same in those experiments[30].) This explains why field enhancement is very low for nanotips even for the sharpest possible tip radii of 10 nm. In addition, the low degree of control over an electrochemically etched tip geometry and other factors cause that nanotip field enhancement results are inconsistent. Therefore, our experiments on plasmonic nanoparticles with highly controlled fabrication and comparison to simulations without fitting parameters aim at the full validation of this methodology.

Based on these considerations, probing nanoplasmonic field enhancement can be performed in the experimental geometry illustrated in Fig. 1. By back-side illuminating a plasmonic sample on a transparent substrate in vacuum and measuring the spectra of photoemitted electrons with a time-of-flight spectrometer, we could accurately determine maximum kinetic energies (Q_{max}) acquired in the rescattering process by evaluating spectral cutoffs (for details, see Fig. 1(c)). Thus, according to Eq. (1), $E_{\mathrm{loc,max}}$ is also given. By characterizing the focal spot, the pulse length and the pulse energy of the laser beam accurately, the peak field strength, $E_{\mathrm{focus,max}}$ can be also inferred for the interaction volume. The measured maximum field enhancement is then given by $E_{\mathrm{loc,max}}/E_{\mathrm{focus,max}}$. In addition to the maximum field enhancement on a given sample, other features of the near fields can not be extracted since both the photoemission phase and the local field enhancement are inherently encoded into the final kinetic energy of a given photoelectron. It is obvious, however, that the highest kinetic energy is gained by rescattering photoelectrons originating from the hottest spot.

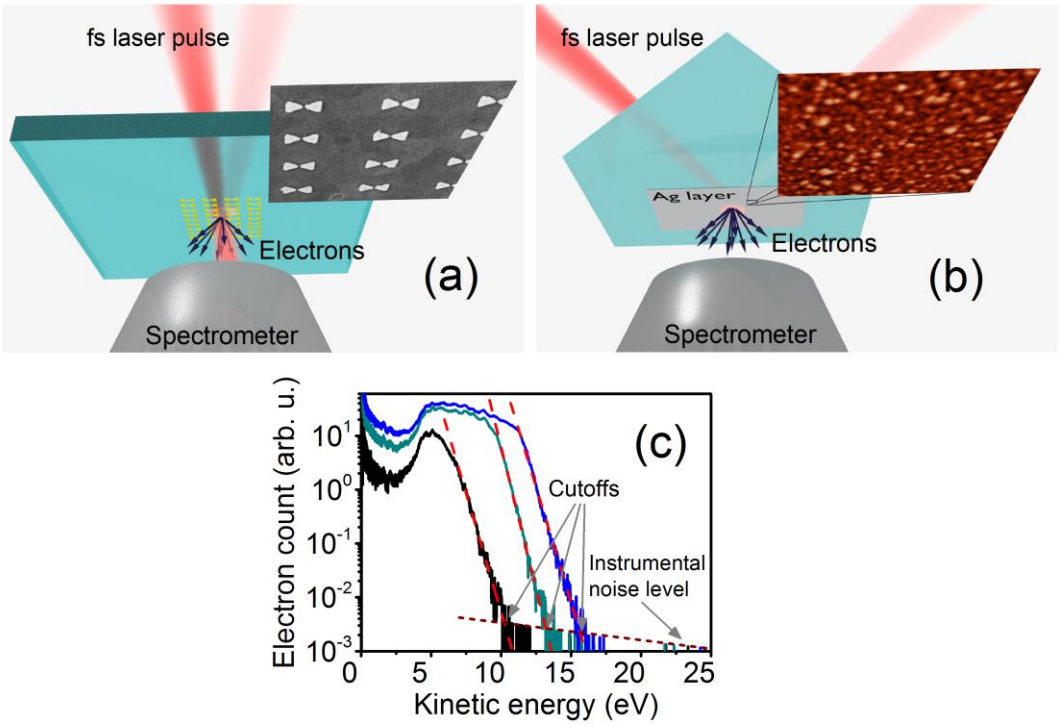

Figure 1. (a) Experimental scheme for measuring photoemission spectra induced by localized plasmon fields at gold nanoparticle arrays. The sample is in vacuum and the substrate is illuminated from the back side through the transparent substrate, so that photoelectrons emitted from the nanoparticles can directly enter a time-of-flight electron spectrometer. (b) Experimental Kretschmann-coupling scheme for measurement of plasmonic photoelectrons from silver layers of some 50 nm thickness exhibiting different surface roughnesses. (c) Typical plasmonic photoelectron spectra. Intersection of the red dashed line fitted to the decaying sections of the spectra and the line fitted to the baseline (instrumental noise floor) define the maximum electron kinetic energy (cutoff).

In order to demonstrate the robustness of our method, we generated both propagating and localized plasmons with femtosecond laser pulses of either 42 fs or 95 fs duration (depending on

the laser source used, see Supporting Information file). The lasers featured 792 and 804 nm central wavelength. Samples supporting localized plasmon oscillations (i.e. arrays of gold plasmonic nanoparticles) were manufactured with standard electron beam lithography onto fused silica substrates with a 40 nm thick indium-tin-oxide (ITO) conductive layer on top (Fig. 1(a)). Nanorods featured 154 nm × 88 nm × 40 nm size, whereas bowties were 89 nm wide, 40 nm thick and the full length of the double triangle together with a 20 nm gap in between them was 260 nm. In addition, thin film samples with 0.7 and 4.7 nm root-mean-square (rms) roughness (Fig. 1(b)) were produced for Kretschmann-type coupling by electron beam evaporation of Ag with precisely controlled temperature and wetting layers[32,33]. The upper row in Fig. 2 shows scanning electron microscope (SEM) and atomic force microscope (AFM) images of the samples. The plasmonic properties of the samples were characterized either by optical spectroscopy (nanoparticles) or by measuring the angular surface plasmon coupling resonance of the thin films (Fig. 2, second row).

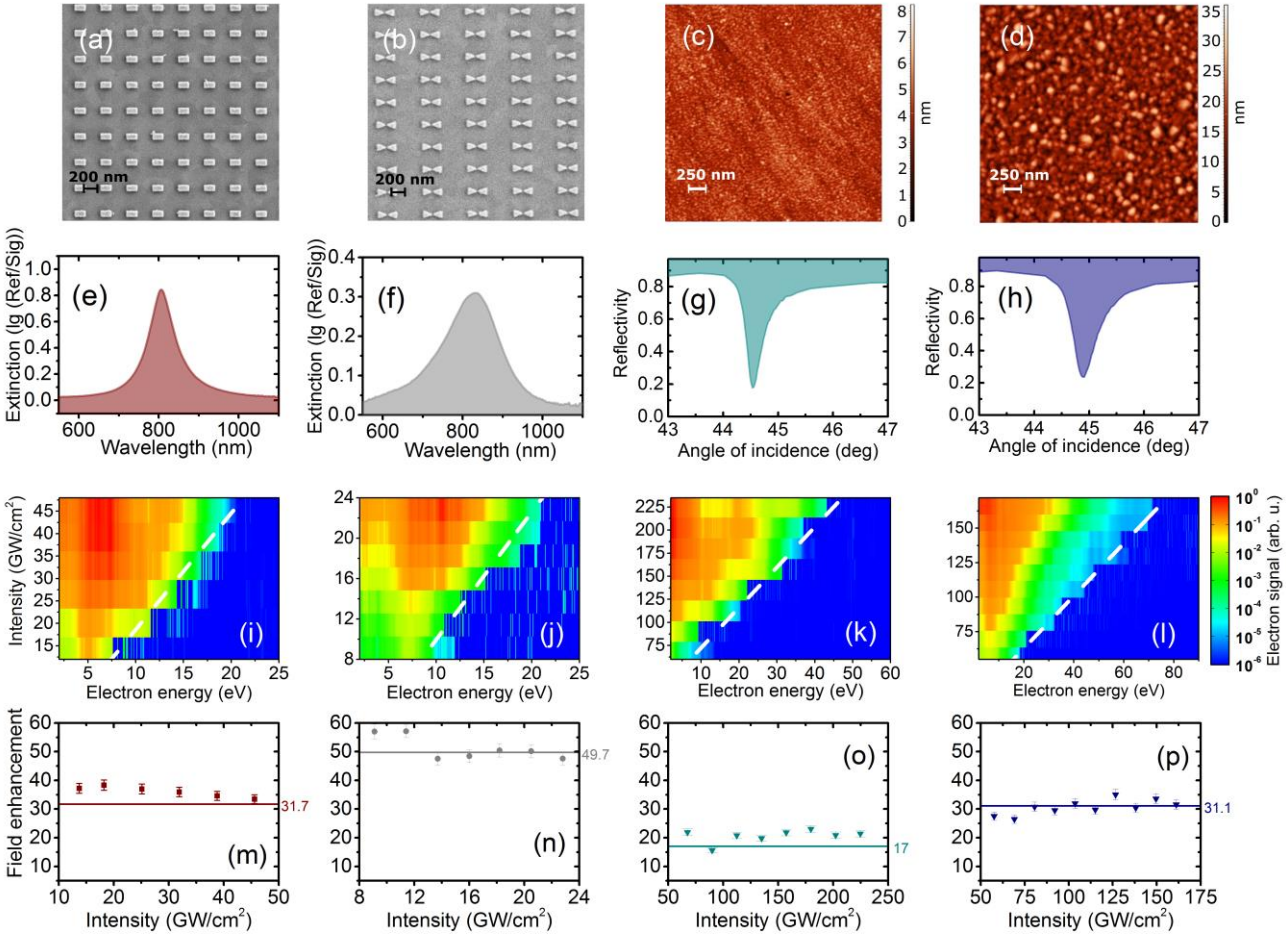

Figure 2. (a), (b) SEM images of plasmonic nanoparticle samples and (c), (d) AFM images of rough plasmonic films used for the measurement of field enhancement. (e), (f) Measured spectral resonance (extinction) curves of the nanoparticles corresponding to (a) and (b), respectively. (g), (h) Measured angular resonance curves of propagating plasmons at 804 nm wavelength, according to the geometry in Fig. 1(b). (i)-(l) Plasmonic photoemission electron spectra as a function of focused laser intensity for the corresponding samples plotted in logarithmic false color representation. The white dashed lines show the linear dependence of the spectral cutoffs. (m)-(p) Maximum plasmonic field enhancement values extracted from the electron spectral cutoffs

according to Eq. (1), as a function of intensity for the corresponding samples. The horizontal lines show the simulated field enhancement values.

We acquired time-of-flight electron spectra for different laser intensities for each sample type by collecting the photoemitted electrons according to the geometry in Fig. 1 with the electron spectrometer having an acceptance cone of 37° (full cone angle). Logarithmically color-coded electron spectra as a function of intensity are shown in the third row in Fig. 2. For each sample, the validity of ansatz (iii) and equation (1) is clearly visible by observing the linear scaling of the cutoff electron energies (marked with white dashed lines) with the focused laser intensity (being proportional to $E^2_{\mathrm{loc,max}}$). Field enhancement factors extracted with the procedure described above are also depicted as a function of laser intensity in the bottom row of Fig. 2. It can be seen that the measured maximum field enhancement values correspond to initial expectations. In particular, we find higher values for localized plasmon resonances than for film surface plasmons, with the highest values observed for the bowtie structure.

In order to validate experimentally measured field enhancement values, we modeled localized and propagating plasmon generation, exactly reproducing the experimental conditions. For these simulations, the FDTD Solutions software package by Lumerical Inc. was used. The simulated 3D unit cell in case of localized plasmonic fields contained a 40 nm thick gold structure with rounded edges. (Radii of curvature were 8.75 nm for nanorods as well as 11 nm for bowties, based on the evaluation of curvature distributions on SEM images. For more details see the Supporting Information.) Nanoparticles were placed on top of a bulk fused silica substrate covered with an ITO layer (see Figs. 3(a) and (b)). A linearly polarized plane wave source with 800 nm central wavelength was applied to illuminate the nanostructure arrays from the substrate side. After carrying out a numerical convergence study on the nanostructure meshing (see

Supporting Information), field distributions recorded near the apices (Figs. 3(c) and (d)) were used to determine the maximum field enhancement values for those planes from which the electrons can reach the detector. In Figs. 3(c) and (d), the color bar shows directly the field enhancement values since the field amplitude of the incident laser pulse was set to be unity.

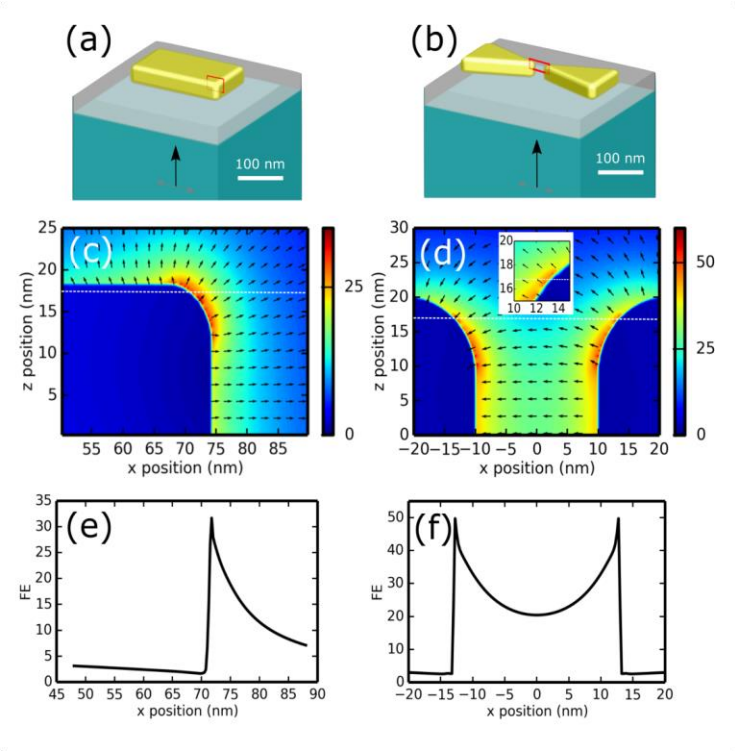

Figure 3. (a) and (b) Scheme of the simulated nanorod and the bowtie structures with 8.75 nm and 11 nm radius-of-curvature at the edges, respectively. (These values were determined from the corresponding distributions on SEM images). The black arrow shows the incidence of a linearly polarized plane wave with the polarization direction indicated by the grey arrows. Grey areas indicate the 40-nm indium-tin-oxide layer whereas blue indicates the fused silica substrate. The red rectangles show the areas of the field distribution maps in (c) and (d); the maximum field enhancement near the apices of the nanorod and the bowtie particles reaches maximum values of 31.7 and 49.7, respectively. Arrows with normalized lengths in (c) and (d) indicate field

vectors showing that for the hottest spots, the field vectors are between 35° and 50° with respect to the substrate plane. (e) and (f) are field enhancement profiles along the sections marked with white dashed lines in (c) and (d).

For modeling the rough surfaces, representative areas with 300 nm × 300 nm lateral size (containing representative surface grains) were chosen from each AFM image recorded on the samples. These images were directly imported to the software to model the 0.7 nm and 4.7 nm rms roughness silver surfaces on a fused silica substrate (Figs. 4 (a) and (b)). After confirming numerical convergence with respect to the mesh density in the simulations, the field distribution recorded for optimal plasmon coupling is presented in Fig. 4 (c) and (d) in planes showing the largest field enhancement values.

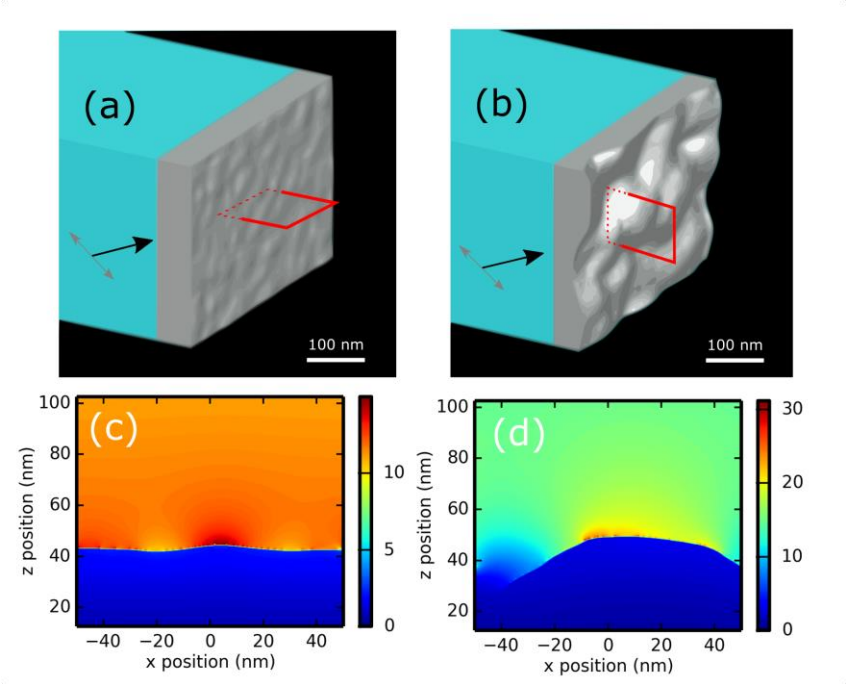

Figure 4. (a) and (b) Scheme of the modeled silver surfaces with two different roughness values. The black arrows show the incidence of a linearly polarized plane wave with the polarization direction indicated by the grey double arrows. The red

rectangles show the areas of representative surface grains where field distributions were recorded, as shown in (c) and (d). The surfaces were selected from AFM images and we picked those portions which contained the most representative grains (being at the maximum of grain size distributions, see Supporting Information). Maximum field enhancement values of 17.0 and 31.1 are found for angles of incidence of 44.6°and 44.8°, respectively, corresponding to the optimum surface plasmon excitation conditions.

We sum up all measured and simulated results in Table 1, showing maximum field enhancement values, including experimental error intervals for our four different samples. We also defined standard deviation for our numerical data based on the distribution of the radii of curvature that can be observed in the nanoparticle ensemble of the array, and the grain size distribution for rough silver surfaces (see Supporting Information).

Table 1. Measured and simulated maximum field enhancement values for four different localized and propagating plasmon samples corresponding to Figs. 2(a-d), respectively.

Sample name	**Corresponding figures**	**Maximum measured field enhancement factor**	**Maximum simulated field enhancement factor**
Resonant gold nanorod	2(a), 3(c)	36.1 ± 1.7	31.7 ± 5.3
Resonant gold bowtie	2(b), 3(d)	50.5 ± 4.0	49.7 ± 5.8
Silver film with 0.7 nm roughness	2(c), 4(c)	21.0 ± 2.4	17.0 ± 1.3
Silver film with 4.7 nm roughness	2(d), 4(d)	30.8 ± 2.4	31.1 ± 6.4

The close correspondence between measured and simulated maximum field enhancement values confirms the validity of this new nanoplasmonic characterization method. The marked

differences between nanorod/bowtie and smooth surface/rough surface field enhancements are well reproduced in every case. However, it can be seen that deviations between measured and simulated field enhancement values for different sample types can be as much as 23 %. We expect to improve the accuracy of our method by considering the complex refractive indices of the materials involved with higher accuracy. For the silver plasmonic films, we had concrete permittivity measurement data for samples prepared in an identical way[32,33], therefore we used $\varepsilon' = -30.07$ and $\varepsilon'' = 1.98$ for the smoother surface and $\varepsilon' = -30.07$ and $\varepsilon'' = 0.90$ for the rougher surface. For gold nanoparticles $\varepsilon' = -22.89$ and $\varepsilon'' = 0.75$ was used[34]. In addition, more sophisticated electron spectroscopic techniques (offering a higher dynamic range for more precise maximum kinetic energy measurement) and better sample homogeneity will enable us to improve the measurement precision in the near future. Nevertheless, current data and accuracy level of this novel method already prove the robustness of this nanoscale field measurement approach.

In summary, we proposed, demonstrated and validated a novel experimental approach for measuring the maximum nanoplasmonic field enhancement at any nanostructured surface. Measured data show good agreement with FDTD simulations for four different plasmonic geometries involving both propagating and localized surface plasmons. We expect that by using advanced electron spectroscopic tools involving spatial and/or k-space resolution, as well, the accuracy of this method can be further improved and laterally resolved nanoscale field mapping will become possible. Our results establish ultrashort-pulse-induced plasmonic photoelectrons as versatile probes for nanoplasmonic near-fields, offering applications in most research fields of contemporary plasmonics.

Supporting Information. Experimental methods and quiver amplitude calculations of electrons in the nanooptical near-fields are provided. Further details of the finite-difference time-domain simulations are also given, including radius-of-curvature evaluation for nanoparticle edges and corners, grain size distributions for the rough films, rough nanoparticle simulations and FDTD convergence studies. This material is available free of charge via the Internet at http://pubs.acs.org.

AUTHOR INFORMATION

Corresponding Author

*E-mail: dombi.peter@wigner.mta.hu

Author Contributions

P. D. conceived the experiments, coordinated the research and wrote the manuscript. Sample design, fabrication and optimization were provided by P. W., T. S., C. P. and J. R. K. P. R., I. M. and P. D. performed the experiments and analyzed data, Z. P. and J. B. conceived and performed the simulations and wrote corresponding paragraphs. All authors contributed to and have given approval to the final version of the manuscript.

‡These authors contributed equally.

Funding Sources

1. Hungarian Academy of Sciences ("Lendület" Grant, Ultrafast Nanooptics).

2. National Research, Development and Innovation Office of Hungary (projects 109257 and 109472).

3. COST Action MP1302 "Nanospectroscopy".

4. Max Planck Society, Partner Group Grant ("Ultrafast strong-field nanoplasmonics").

Notes

The authors declare no competing financial interests.

ACKNOWLEDGMENT

We acknowledge fruitful discussions with Győző Farkas and Norbert Kroó as well as Viktor Ayadi for continued computing support. The authors acknowledge the Hungarian Academy of Sciences ("Lendület" Grant, Ultrafast Nanooptics) and the National Research, Development and Innovation Office of Hungary (projects 109257 and 109472) for financing this research. Financial support by the European Cooperation in Science and Technology through COST Action MP1302 Nanospectroscopy is gratefully acknowledged. Partial support by the ELI-ALPS project is also acknowledged. The ELI-ALPS project (GOP-1.1.1-12/B-2012-000, GINOP-2.3.6-15-2015-00001) is supported by the European Union and co-financed by the European Regional Development Fund. We also acknowledge the Max Planck Society for support in the form of a Partner Group Grant.

REFERENCES

(1) Atwater, H. A. *Sci. Am.* **2007**, 296, 56–63.

(2) Schuller, J. A.; Barnard, E. S.; Cai, W., Jun, Y. C.; White, J. S.; Brongersma, M. L. *Nat. Mater.* **2010**, 9, 193–204.

(3) Campion, A.; Kambhampati, P. *Chem. Soc. Rev.* **1998**, 27, 241-250.

(4) Willets, K. A.; Van Duyne, R. P. *Annu. Rev. Phys. Chem.* **2007**, 58, 267-297.

(5) Anker, J. N.; Hall, W. P.; Lyandres, O.; Shah, N. C.; Zhao, J.; Van Duyne, R. P. *Nat. Mater.* **2008** 7, 442-453.

(6) Homola, J.; *Chem. Rev.* **2008**, 108, 462–493.

(7) Koller, D. M.; Hohenau, A.; Ditlbacher, H.; Galler, N.; Reil, F.; Aussenegg, F. R.; Leitner A.; List, E. J. W.; Krenn, J. R. *Nat. Photonics* **2008**, 2, 684-687.

(8) Falk, A. L.; Koppens, F. H. L.; Yu, C. L.; Kang, K.; de Leon Snapp, N.; Akimov, A. V.; Jo, M.-Ho.; Lukin, M. D.; Park H. *Nat. Phys.* **2009**, 5, 475-479.

(9) Ferry, V. E.; Sweatlock, L. A.; Pacifici, D.; Atwater, H. A. *Nano Lett.* **2008**, 8, 4391–4397.

(10) Tsujino, S.; Beaud, P.; Kirk, E.; Vogel, T.; Sehr, H.; Gobrecht, J.; Wrulich, A. *Appl. Phys. Lett.* **2008**, 92, 193501.

(11) Li, R. K.; To, H.; Andonian, G.; Feng, J.; Polyakov, A.; Scoby, C. M.; Thompson, K.; Wan, W.; Padmore, H. A.; Musumeci P. *Phys. Rev. Lett.* **2013**, 110, 074801.

(12) Vogelsang, J.; Robin, J.; Nagy, B. J.; Dombi, P.; Rosenkranz, D.; Schiek, M.; Groß, P.; Lienau C. *Nano Lett.* **2015**, 15, 4685–4691.

(13) Hobbs, R. G.; Yang, Y.; Fallahi, A.; Keathley, P. D.; De Leo, E; Kärtner, F. X.; Graves, W. S.; Berggren, K. K. *ACS Nano* **2014**, 8, 11474-11482.

(14) Stockman, M. I. *Opt. Express* **2011**, 19, 22029-22106.

(15) Fang, Y.; Seong, N.-H.; Dlott, D. D. *Science* **2008**, 321, 388-392.

(16) Rycenga, M.; Xia, X.; Moran, C. H.; Zhou, F.; Qin, D.; Li, Z.-Y.; Xia, Y. *Angew. Chem., Int. Ed. Engl.* **2011**, 50, 5473–5477.

(17) Schuck, P. J.; Fromm, D. P.; Sundaramurthy, A.; Kino, G. S.; Moerner, W. E. *Phys. Rev. Lett.* **2005**, 94, 017402.

(18) Sundaramurthy, A.; Schuck, P. J.; Conley, N. R.; Fromm, D. P.; Kino, G. S.; Moerner, W. E. *Nano Lett.* **2006**, 6, 355-360.

(19) Deeb, C.; Bachelot, R.; Plain, J.; Baudrion, A.-L.; Jradi, S.; Bouhelier, A.; Soppera, O.; Jain, P. K.; Huang, L.; Ecoffet, C.; Balan, L.; Royer, P. *ACS Nano* **2010**, 4, 4579–4586.

(20) Geldhauser, T.; Kolloch, A.; Murazawa, N.; Ueno, K.; Boneberg, J.; Leiderer, P.; Scheer, E.; Misawa, H. *Langmuir* **2012**, 28, 9041−9046.

(21) Harrison, R. K.; Ben-Yakar A. *Opt. Express* **2010**, 18, 22556-22571.

(22) Ward, D. R.; Hüser, F.; Pauly, F.; Cuevas, J. C.; Natelson, D. *Nature Nanotechnol.* **2010**, 5, 732-736.

(23) Tsang, T.; Srinivasan-Rao, T.; Fischer, J. *Phys. Rev. B* **1991**, 43, 8870-8878.

(24) Zawadzka, J.; Jaroszynski, D. A.; Carey, J. J.; Wynne, K. *Appl. Phys. Lett.* **2001**, 79, 2130-2132.

(25) Kupersztych, J.; Monchicourt P.; Raynaud, M. *Phys. Rev. Lett.* **2001**, 86, 5180-5183.

(26) Dombi, P.; Hörl, A.; Rácz, P.; Márton, I.; Trügler, A.; Krenn, J. R.; Hohenester, U. *Nano Lett.* **2013**, 13, 674−678.

(27) Grubisic, A.; Ringe, E.; Cobley, C. M.; Xia, Y.; Marks, L. D.; Van Duyne, R. P.; Nesbitt, D. J. *Nano Lett.* **2012**, 12, 4823–4829.

(28) Paulus, G. G.; Nicklich, W.; Xu, H.; Lambropoulos, P.; Walther, H. *Phys. Rev. Lett.* **1994**, 72, 2851-2854.

(29) Busuladžić, M.; Gazibegović-Busuladžić, A.; Milošević D. B. *Laser Phys.* **2006**, 16, 289–293.

(30) Thomas, S.; Krüger, M.; Förster, M.; Schenk, M.; Hommelhoff, P. *Nano Lett.* **2013**, 13, 4790-4794.

(31) Herink, G.; Solli, D. R.; Gulde, M.; Ropers C. *Nature* **2012,** 483, 190-193.

(32) Stefaniuk, T.; Wróbel, P.; Trautman, P.; Szoplik T. *Appl. Opt.* **2014**; 53, B237-B241.

(33) Wróbel, P.; Stefaniuk, T.; Trzcinski, M.; Wronkowska, A. A.; Wronkowski, A.; Szoplik, T. *ACS Appl. Mater. Interfaces* **2015**, 7, 8999–9005.

(34) Haynes, W. M. (Ed.): *CRC Handbook of Chemistry and Physics, 96th Edition*, CRC Press Taylor and Francis Group, Boca Raton FL, **2015**.